Nonlinear Dynamics of Interband Cascade Laser Subjected to Optical Feedback

Han, Hong; Cheng, Xumin; Jia, Zhiwei; Shore, K. Alan

Photonics

DOI:
10.3390/photonics8090366

Published: 01/01/2021

photonics

MDPI

Article

Nonlinear Dynamics of Interband Cascade Laser Subject to Optical Feedback

Hong Han[1,*], Xu Min Cheng[1] and K. Alan Shore[2]

is [1] Key Laboratory of Advanced Transducers and Intelligent Control System, Ministry of Education, College of Physics and Optoelectronics, Taiyuan University of Technology, Taiyuan 030024, China; hanhong@tyut.edu.cn
[2] School of Electronic Engineering, Bangor University, Wales, LL57 1UT, UK; k.a.shore@bangor.ac.uk
* Correspondence: hanhong@tyut.edu.cn

Abstract: We present a comprehensive study of the nonlinear dynamics of long external cavity delayed optical feedback induced interband cascade lasers(ICL). Using the modified Lang-Kobayashi equations, we numerically investigate the effects of some key parameters on the first Hopf bifurcation point of ICL with optical feedback, such as delay time(τ_f), pump current(I), linewidth enhancement factor(LEF), stage number(m) and feedback strength. It is found that compared with τ_f, I, LEF and m have significant effect on the stability of the ICL. Additionally, our results show that for few stage number ICL subject to external cavity optical feedback is more susceptible to exhibiting chaos. The chaos bandwidth dependence on m, I and feedback strength are investigated, and 12 GHz bandwidth mid-infrared chaos is observed.

Keywords: interband cascade laser; mid-infrared chaos; optical feedback; nonlinear dynamics

Citation: Lastname, F.; Lastname, F.; Lastname, F. Title. *Photonics* **2021**, *8*, x. https://doi.org/10.3390/xxxxx

Received: date
Accepted: date
Published: date

1. Introduction

The interband cascade laser(ICL) as a mid-infrared semiconductor laser has made significant progress in the last two decades[1-6]. The RAND Corporation reports that mid-infrared lasers in the 3-5 μm band of the atmospheric transmission window have good atmospheric transmission characteristics, lower transmission losses than other bands, and is less susceptible to weather factors[7]. In addition, the mid-infrared band covers the absorption peaks of many atoms and molecules[8]. Therefore, it can be used in applications such as gas detection[9,10], clinical respiratory diagnosis[11] and free-space optical communication[12].

In contrast to Quantum cascade lasers (QCLs), the ICL is a bipolar device with the electronic transition of the ICL occuring between the conduction band and the valence band[13]. Therefore, the carrier lifetime of ICL is of nanosecond order as in more conventional semiconductor lasers. Also in recent experimental reports the linewidth enhancement factor of ICLs is found to be about 2.2 which is much higher than that of QCLs[14]. Both of these characteristics suggest that when subject to external perturbation the ICL will exhibit rich nonlinear dynamics. Wang Cheng et al.'s recent experiments confirm that with external optical feedback ICL present periodic oscillations and weak chaos[15]. 450 MHz low frequency oscillation (detector bandwidth limited) chaos was observed. However, the route to chaos and the identification of means for obtaining strong chaos are open for detailed study.

In this paper, modified Lang-Kobayashi equations are used to investigate the dynamics of ICL subject to external optical feedback. Considering the spatial length of the light path in many experiments, we focus on the long-cavity optical feedback case , wherein the external feedback time lag is larger than the oscillation relaxation time of the f ICL[16]. The pump current, feedback strength, stage number and linewidth enhancement factor effects on stability of ICL are analyzed, and the influence of *m*, *I* and feedback strength on the bandwidth of chaos.

2. Theoretical model

Figure 1a presents the ICL structure with stage number of 3. Initially the electron transition in the ICL occurs between the first conduction band and the first valence band as indicated as E_e (blue potential well) and E_h (red potential well) in the left upper corner Figure 1a[17]. After the first time electron transition, the electron reaches the second stage conduction band through interband tunneling, and then repeats the electron transition in the second stage and then in the third stage. Figure 1b is the schematic diagram of an ICL subject to external mirror feedback, where τ_f is the feedback time delay.

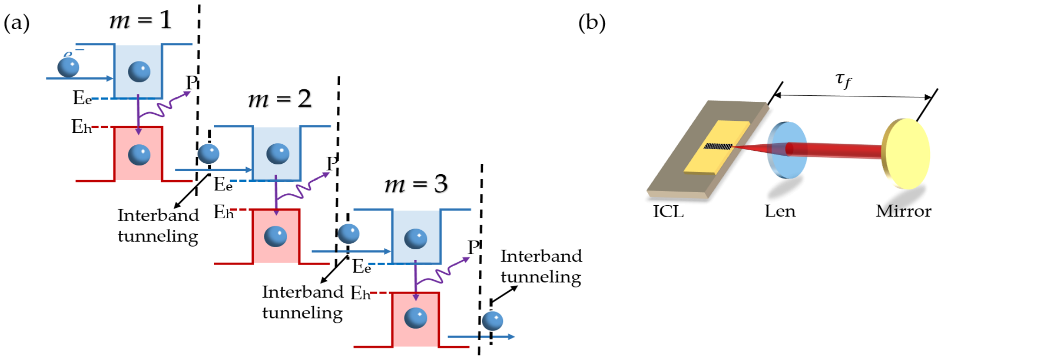

Figure 1. (a) 3 stage number structure of ICL; **(b)** Schematic diagram of ICL with optical feedback structure.

Appropriately modified Lang-Kobayashi equations, by adding an optical feedback term in optical fields, rate equations of ICL with mirror optical feedback are as follows[18,19]

$$\frac{dN(t)}{dt}=\eta\frac{I}{q}-\Gamma_p\upsilon_g gS-\frac{N}{\tau_{sp}}-\frac{N}{\tau_{aug}} \tag{1}$$

$$\frac{dS(t)}{dt}=\left[m\Gamma_g\upsilon_g g-\frac{1}{\tau_p}\right]S(t)+m\beta\frac{N}{\tau_{sp}}+2k\sqrt{S(t)S(t-\tau_f)}cos\theta(t) \tag{2}$$

$$\frac{d\varphi(t)}{dt}=\frac{\alpha_H}{2}\left[m\Gamma_p\upsilon_g g-\frac{1}{\tau_p}\right]-k\sqrt{\frac{S(t-\tau_f)}{S(t)}}sin\theta(t) \tag{3}$$

where $N(t)$, $S(t)$ and $\varphi(t)$ respectively represent carrier number, photon number and phase of the electric field. m is number of the cascade gain stage, τ_{sp} is the spontaneous radiation lifetime and τ_{aug} is the Auger recombination lifetime. Since the Auger recombination lifetime τ_{aug} in ICL is smaller than the spontaneous radiation lifetime τ_{sp}, τaug must be considered in the current-carrying dynamics[20]. η is the current injection efficiency, Γp is the optical confinement factor per gain stage, v_g is the group velocity of light, g is the material gain per stage. τ_p is photon lifetieme, and k is the feedback efficient which is given by $k=2C_l\sqrt{f_{ext}}/\tau_{in}$, where τ_{in} is the internal cavity roundtrip time, f_{ext} is the feedback strength which is defined as the power ration between the feedback light and the laser output, and C_l is an external coupling coefficient. The external coupling coefficient can be expressed as C_l=$(1-R)/2\sqrt{R}$, with R is the reflection coefficient of the laser front facet facing the external mirror.

The steady-state solutions for the ICL operating above the threshold current are as follows[19]

$$N = \frac{1}{m}\frac{A}{\Gamma_p v_g a_0 \tau_p} + N_{tr} \tag{4}$$

$$S = m\eta\tau_p \frac{I - I_{th}}{q} \tag{5}$$

$$I_{th} = \frac{q}{\eta}\left(\frac{1}{m}\frac{A}{\Gamma_p v_g a_0 \tau_p} + N_{tr}\right)\left(\frac{1}{\tau_{sp}} + \frac{1}{\tau_{aug}}\right) \tag{6}$$

The descriptions of other symbols and the selected values for simulation are shown in Table 1, as taken from[14,17,19-22]. The integral time lag in the simulation is 0.1ps.

Table 1. ICL parameters used in the simulations.

Parameter	Symbol	Value
Cavity length	L	2mm
Cavity width	W	4.4μm
Group velocity of light	v_g	8.38×10^7m/s
Wavelength	λ	3.7μm
Active area	A	8.6×10^{-9}m^2
Facet reflectivity	R	0.32
Refractive index	n_r	3.58
Optical confinement factor	Γ_p	0.14
Stage number	m	5,10
Injection efficiency	η	0.64
Photon lifetime	τ_p	10.5ps
Spontaneous emission time	τ_{sp}	15ns
Auger lifetime	τ_{aug}	1.08ns
Threshold current	I_{th}	16.6mA (*m*=5)
Feedback strength	f_{ext}	0~60%
Time delay	τ_f	1~3ns
Differential dain	α_0	2.8×10^{-10}cm
Transparent carrier number	N_{tr}	6.2×10^7
Spontaneous emission factor	β	1×10^{-4}
Linewidth enhancement factor	α_{H}	2.2

3. Numerical results

We calculate the carrier numbers and photon numbers as bias current increases as shown in Figure 2a and 2b, respectively. It is found that stage number *m* has little effect on carrier numbers(in Figure 2a) but it influences photon numbers(in Figure 2b). For relative large stage numbers such as *m*=10, the output power is much higher than the case *m*=5(black) as shown in Figure 2b.

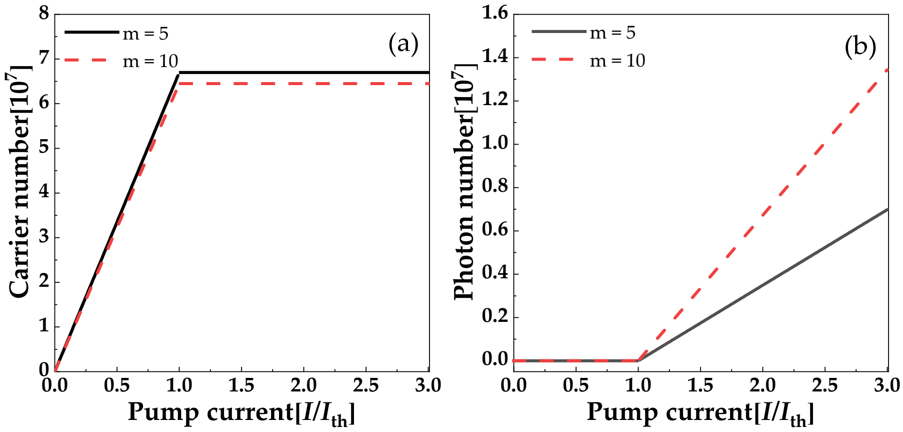

Figure 1. Carrier number **(a)** and photon number **(b)** vs. pump current. Black solid and red dashed curves present stage number m=5 and m=10 respectively.

3.1. Route to chaos

Figure 3 shows the output of the ICL with external optical feedback as the feedback strength increases, for the case m = 5. The ICL output is stable when the feedback strength f_{ext} ranges from 0 (i) to 0.07%. Without feedback, that is f_{ext}=0, the relaxation oscillation frequency f_R can be observed from RF spectrum (d-i) to be 1.79 GHz. This is in accordance with the value 1.794 GHz obtained by calculating the relaxation oscillation frequency via the relation f_R=1/[2π(G_0S/τ_p)$^{-1/2}$], where G_0=$\Gamma_p v_g a_0$/A. As the feedback strength increases the ICL enters into period-1 dynamics (ii), quasi-periodic dynamics (iii), multiple-period oscillations (iv), then displays chaos (v). The frequency of period-1 oscillations is 1.85GHz as shown in Figure 3(d-ii), which is little larger than the relaxation oscillation frequency of the ICL. As the feedback strength increases, quasi-periodic oscillation is found, which is confirmed by RF spectrum and phase diagram, that is more frequencies are induced in Figure 3(d-iii) and more loops are found in the phase in Figure 3(c-iii), respectively. Also multiple-period dynamics is observed as shown in Figure 3(a-iv) to Figure 3(e-iv). For further Feedback strength increase more complex nonlinear dynamics is introduced hence achieving mid-infrared optical chaos, as shown in Figure 3(a- v) to 3(e-v). In the optical spectra of the chaos shown in Figure 3(e-v), many external cavity modes are found. This can be confirmed from the auto-correlation functions shown in Figure 3(b-v), where the sidelobe peak is at 2.4 ns corresponding to cavity length 36 cm.

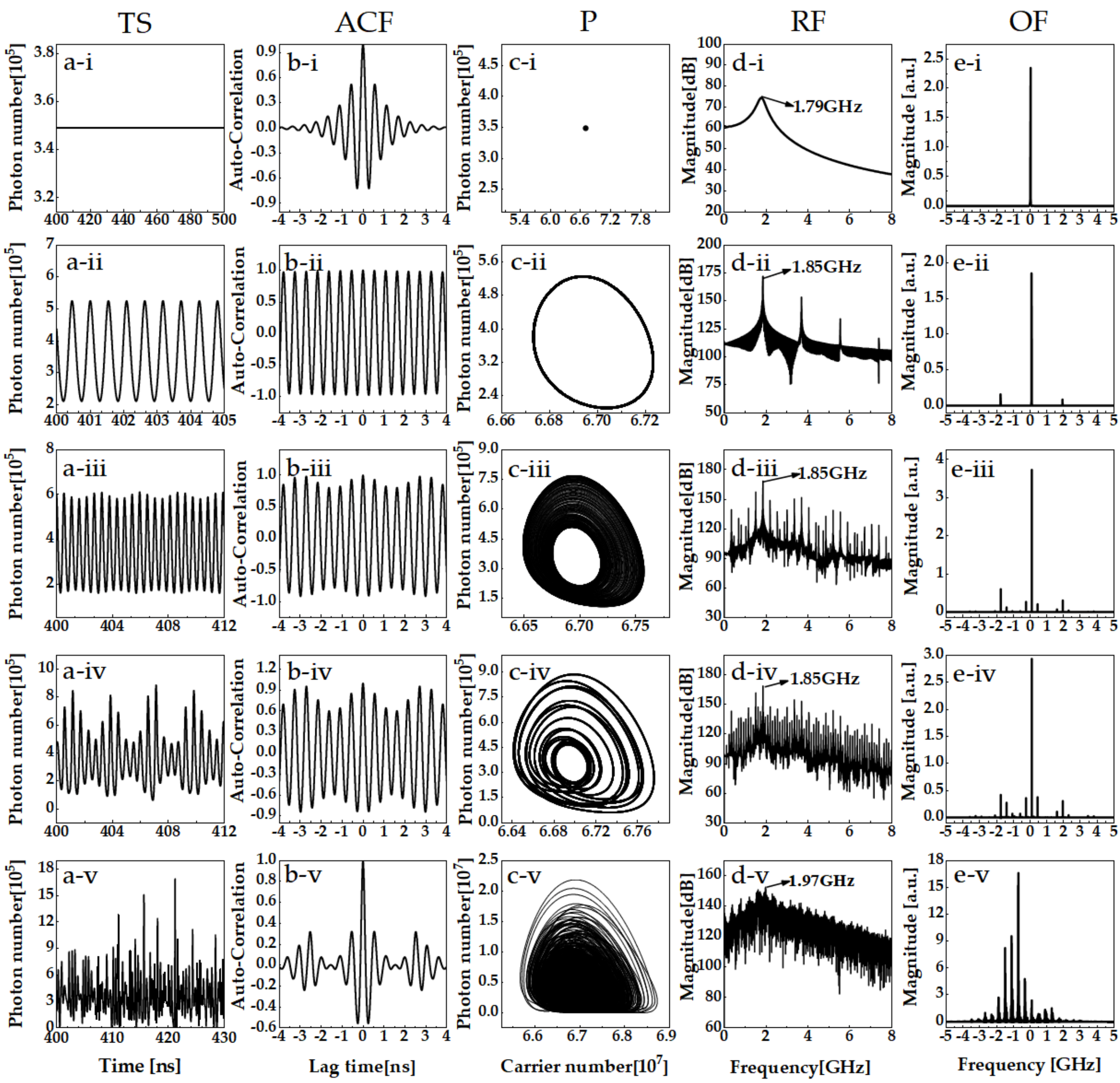

Figure 3. Output of ICL with external optical feedback as feedback strength increases with m=5, I=1.1I_{th}, and τ_f=2.4 ns; from the top down, I: f_{ext}=0.0%, ii: f_{ext}=0.1%, iii: f_{ext}=0.17%, iv: f_{ext}=0.3%, v: f_{ext}=3%; columns **(a)**-**(e)** are time series(TS), autocorrelation curves(ACF), phase portrait(P), radio-frequency spectrum(RF) and optical spectra(OS), respectively.

By using bifurcation diagrams, the dynamics of ICL as feedback strength increasing can be obtained as shown in (a-i) with m=5 and (b-i) with m=10. Maximum Lyapunov exponents can be used to determine whether the ICL output with external optical feedback is chaos (red) or not (blue) as shown in Figure 4(a-ii) and 4(b-ii). As shown in Figure 4(b-i), the route to chaos for a 10-stage ICL with external optical feedback is from stable state to period-1, then quasi-period and then chaos. This route is different from that of a 5-stage ICL where multiple-period oscillations are not observed. This shows that stage number m impacts the route to chaos of an ICL subject to optical feedback.

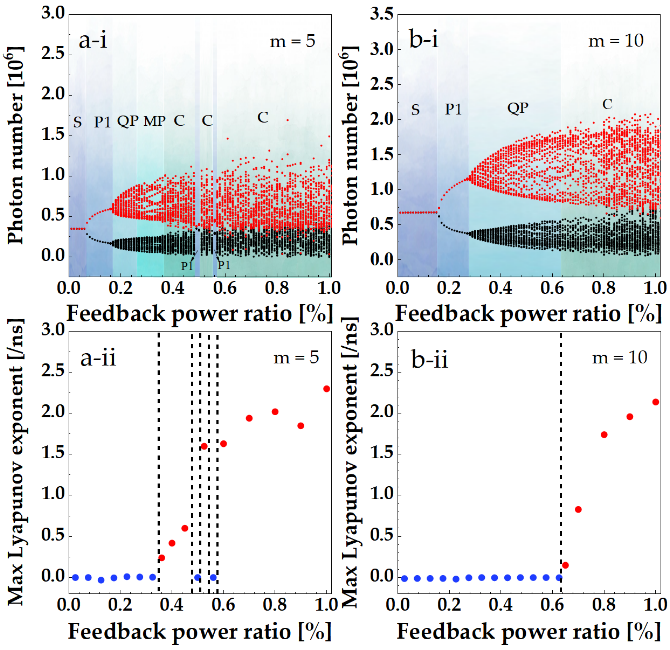

Figure 4. Bifurcations(i) and Max Lyapunov exponents(ii) of ICL with external optical feedback under I=1.1I_{th}, τ_f=2.4 ns. **(a)**: m=5, **(b)**: m=10.

3.2. *Hopf bifurcation analysis*

In this section, we explore the stability of ICLs with external optical feedback. We first compare two stage numbers which are m=5 and m=10 to reveal the effects of time delay, bias current and linewidth enhancement factor on the Hopf bifurcation points. Then ascertain how the Hopf bifurcation changes for stage numbers m in the range 1 to 20.

The pump current is set a little above threshold current, that is 1.1I_{th}. Figure 5. Shows that the external cavity delay has little effects on Hopf bifurcation point values . As the external cavity delay increases from 1.0 ns to 3.0 ns, the Hopf bifurcation point values, that is feedback power ratio for ICL enters into period-1, are in around 0.05% to 0.7%. There is a jump value for τ_f =1.2 ns, in which case f_{ext} =1.2%.

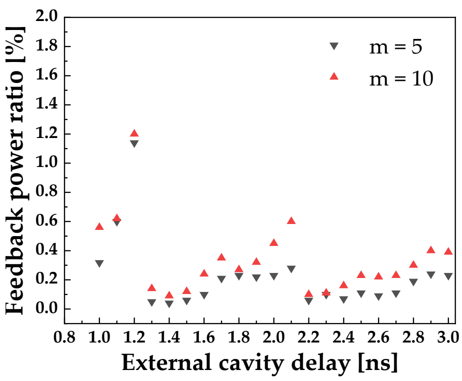

Figure 5. Hopf bifurcation points vs. time delay τ_f for I=1.1I_{th}

To illustrate pump current effects, the Hopf bifurcation points versus bias currents are investigated. In Figure 6a and 6b, two external cavity delays are compared, viz τ_f =1.2 ns and τ_f =2.4 ns. As the pump current increases the Hopf bifurcation point gradually increases, in both m=5 (squares) and m=10 (circles) cases, as well as τ_f =1.2 ns and τ_f=2.4 ns. Compared with τ_f =2.4 ns, τ_f =1.2 ns needs larger feedback power ratio to enable the

ICL to enter into unstable state, which is around 1.4 times of that of τ_f =2.4 ns at pump current is $3I_{th}$. Since these two delays for Hopf bifurcation point values versus bias currents have similar trends, we focus our attention on τ_f =2.4 ns in the following results.

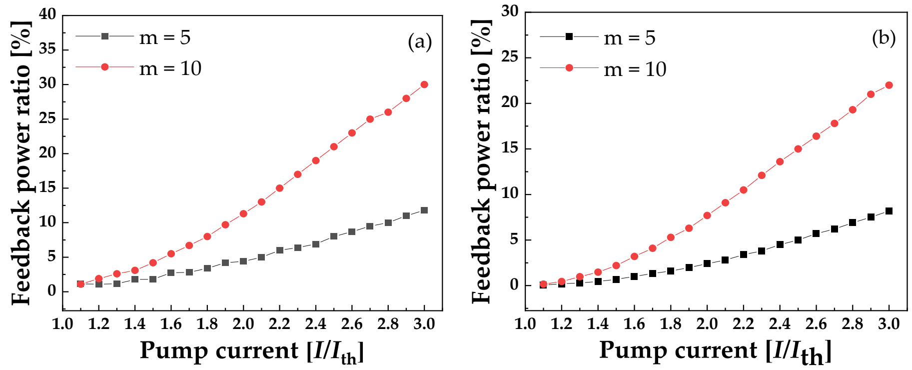

Figure 6. Hopf bifurcation points vs. bias currents. **(a)**: τ_f =1.2 ns**, (b)**: τ_f=2.4 ns.

It is well appreciated that the linewidth enhancement factor, α_H, plays a crucial role in semiconductor laser nonlinear dynamics. For common quantum well laser diodes, α_H is in the range of 2.0 to 5.0. Recent report shows that the below-threshold linewidth enhancement factor of ICL is in the range of 1.1-1.4. Here we calculate Hopf bifurcation points versus linewidth enhancement factor which ranges from 1 to 5, as shown in Figure 7. As the linewidth enhancement factor increases from 1 to 2, the Hopf bifurcation point value reduces rapidly, and then it tends to be stable as α_H increases further. Thus small α_H imparts the ICL with considerable dynamic stability.

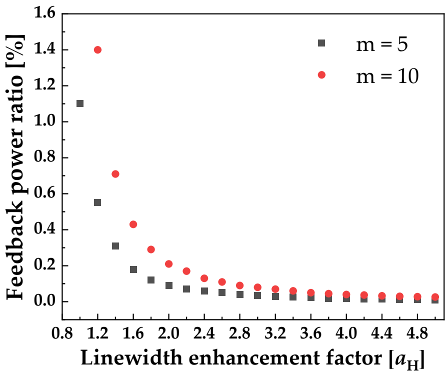

Figure 7. Hopf bifurcation points vs. linewidth enhancement factor under I=1.1I_{th}, τ_f =2.4 ns.

For ICLs the cascade stage number m usually less than 20. Figure 8 shows Hopf bifurcation point values versus stage numbers with I=1.5I_{th}, τ_f=2.4ns. It is seen that as the stage number increases, Hopf bifurcation point values exponentially increases.

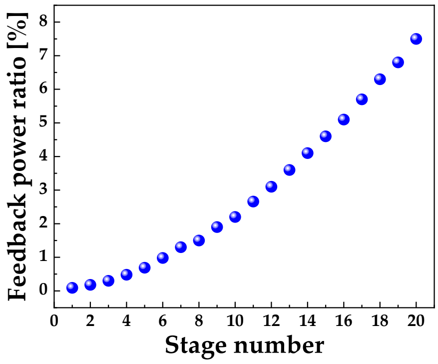

Figure 8. Hopf bifurcation points values vs. stage numbers m with I=1.5I_{th}, τ_f=2.4 ns.

3.1. Bandwidth of Chaos

A broadband RF spectrum is one of the significant characteristics of chaos. By using 80% power energy bandwidth measurement, we investigate the bandwidth of chaos. Similarly to regular quantum well laser diodes, the bandwidth of chaos from ICL with external optical feedback increases as the feedback power ratio increases , as shown in Figure 9.

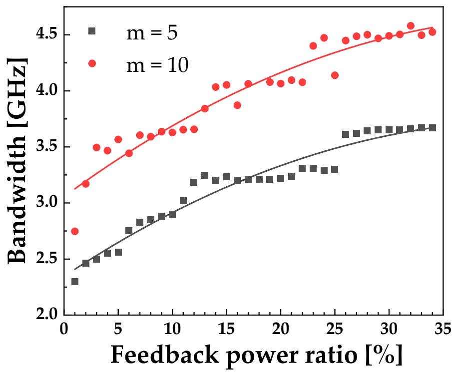

Figure 9. Bandwidth of chaos vs. feedback power ratio under I=1.1I_{th}, τ_f=2.4 ns, m=5 (black squares) and m=10(red circles).

Increasing the pump current is expected to enhance the bandwidth of chaos and is confirmed here in Figure 10. Here, we notice that mid-infrared chaos from ICL has same regularity. Once the pump current increases to 2.2I_{th}, a 10 GHz chaos bandwidth is obtained when the stage number is 10, as shown in Figure 10. That is because occupying main energy frequency component is relaxation frequency oscillation f_R increasing as pump current.

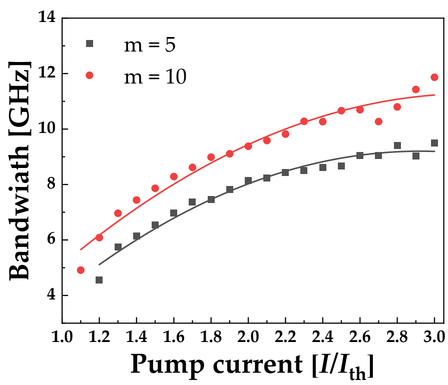

Figure 10. Bandwidth of chaos vs. bias current when feedback power ratio is 60% and τ_f =2.4 ns with *m*=5 (black squares), *m*=10(red circles).

Figure 11 respectively present time series, auto-correlation, phase diagram, RF spectrum and optical spectral of mid-infrared chaos for *m*=5 (in Figure 11a) and *m*=10 (in Figure 11b). This indicates that for relative high stage number the bandwidth of chaos from ICL is further enhanced as shown in Figure 11(a-iv) and (b-iv).

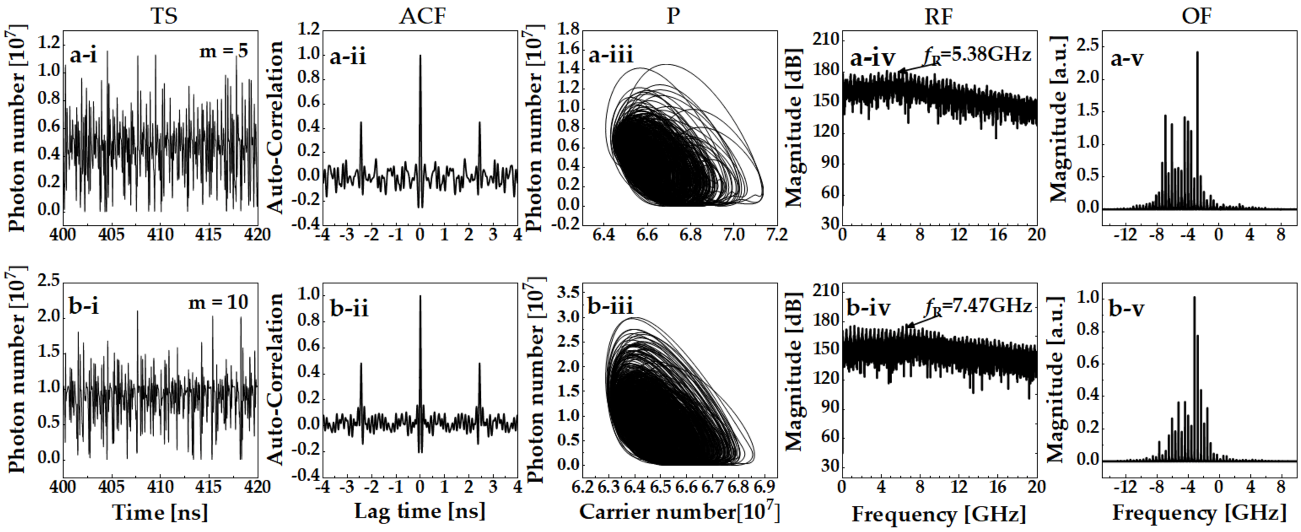

Figure 11. Output chaos of ICL with external optical feedback as stage number increases with I=1.9I_{th}, τ_f =2.4 ns and f_{ext}=60%. **(a)**: *m*=5, **(b)**: *m*=10.

The stage number effect is presented in Figure 12, where *m* ranges from 1 to 20 and pump currents are 1.1I_{th}(black squares) and 2I_{th}(red circles). Although the increase in bandwidth for relative high pump current, 2I_{th}, is faster than that of the relatively low pump current, 1.1I_{th}, the tendency of the stage number effects is the same, that is the bandwidth of chaos increases as the stage number increases. This tendency is verified in Figure 9 to Figure 11.

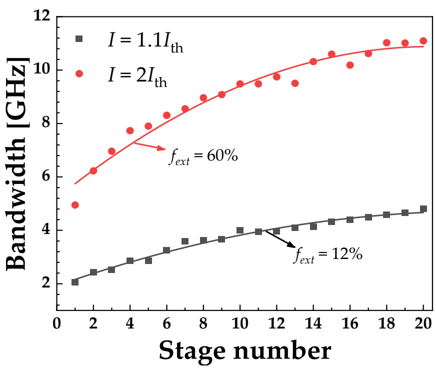

Figure 12. Bandwidth of chaos vs. stage number I=1.1I_{th} (black squares) and I=2I_{th} (red circles) with τ_f =2.4 ns.

By using Max Lyapunov exponents, we distinguish chaos from quasi-period or period-1, and calculate the 80% energy power bandwidth versus feedback power ratio and pump current as shown in Fig. 13. By using dashed curves, we distinguish period-1, quasi-period and chaos and find that as the stage number increases from 5 to 10, the quasi-period region is extended as shown in Fig. 13 (a) and Fig. 13(b). For large stage number, that is

m=10, period-1 is observed when the pump current is above 2.2I_{th}, as indicated in the left upper corner of Fig. 13(b). The boundary of period-1 oscillations in Fig. 13(b) was already presented in Fig. 6(b). Boundary of chaos between quasi-period and chaos reveals that for relative few stage number an ICL with external optical feedback enters into chaos easily as shown in Fig. 3(a). Both of these two stage numbers results confirm that to obtain broadband mid-infrared chaos, one needs relative high pump current as well as large feedback power ratio. Urthermore a 12 GHz bandwidth of mid-infrared chaos can be obtained for m=10 as shown in the right up corner of Fig. 13(b).

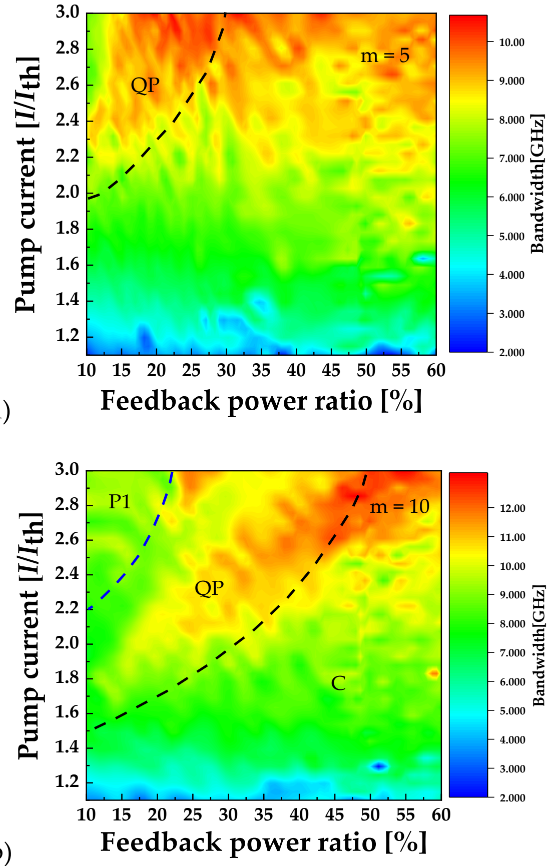

(a)

(b)

Figure 13. Bandwidth vs. feedback power ratio and pump current, with τ_f=2.4 ns. **(a)**: m=5, **(b)**: m=10.

4. Discussion

Authors should discuss the results and how they can be interpreted from the perspective of previous studies and of the working hypotheses. The findings and their implications should be discussed in the broadest context possible. Future research directions may also be highlighted.

5. Conclusions

This section is not mandatory but can be added to the manuscript if the discussion is unusually long or complex.

Author Contributions: Conceptualization, H.H. and K.A.S.; methodology, H.H.; software, X.M.C.; validation, H.H., X.M.C. and K.A.S.; formal analysis, H.H.; investigation, K.A.S..; resources, H.H.;

data curation, X.M.C.; writing—original draft preparation, H.H.; writing—review and editing, K.A.S.; visualization, X.M.C; supervision, H.H.; project administration, H.H.; funding acquisition, H.H. All authors have read and agreed to the published version of the manuscript.

Funding: This research was funded by NATIONAL NATURAL SCIENCE FOUNDATION OF CHINA, grant number 61741512 and 61805168.

Data Availability Statement: The data presented in this study are available on request from the corresponding author.

Acknowledgments: In this section, you can acknowledge any support given which is not covered by the author contribution or funding sections. This may include administrative and technical support, or donations in kind (e.g., materials used for experiments).

Conflicts of Interest: The authors declare no conflict of interest. The funders had no role in the design of the study; in the collection, analyses, or interpretation of data; in the writing of the manuscript, or in the decision to publish the results.

References

1. Lin, C.H.; Yang, R.Q.; Zhang, D.; et al. Type-II interband quantum cascade laser at 3.8 μm. *Electronics Letters Abbrevi* **1997**, *33*, 598-599.
2. Yang, R.Q.; Hill, C.J.; Yang, B.H.; et al. Continuous-wave operation of distributed feedback interband cascade lasers. *Applied Physics Letters* **2004**, 84, 3699-3701.
3. Kim, M.; Canedy, C.L.; Bewley, W.W.; et al. Interband cascade laser emitting at λ=3.75μm in continuous wave above room temperature. *Applied Physics Letters* **2008**, 92, 191110.
4. Canedy, C.L.; Abell, J.; Merritt, C.D.; et al. High-Power CW Operation of 7-Stage Interband Cascade Lasers. *Conference on Lasers & Electro-optics. IEEE* **2014**.
5. Bagheri, M.; Frez, C.; Sterczewski, L.A.; et al. Passively mode-locked interband cascade optical frequency combs. *Scientific Reports* **2018**, 8, 3322.
6. Yang, H.; Yang, R.Q.; He, J.J.; et al. Mid-Infrared Widely Tunable Single-Mode Interband Cascade Lasers Based on V-Coupled Cavities. *Optics Letters* **2020**, 45, 2700-2702.
7. Chen, C.C.; Attenuation of Electromagnetic Radiation by Haze, Fog, Clouds, and Rain. *RAND CORP SANTA MONICA CA* **1975**.
8. Vurgaftman, I.; Weih, R.; Kamp, M.; et al. Interband cascade lasers. *Journal of Physics D Applied Physics* **2005**, 48, 123001.
9. Horstjann, M.; Bakhirkin, Y.A.; Kosterev, A.A.; et al. Formaldehyde sensor using interband cascade laser based quartz-enhanced photoacoustic spectroscopy. *Applied Physics B* **2004**, 79, 799-803.
10. Wysocki, G.; Bakhirkin, Y.; So, S.; et al. Dual interband cascade laser based trace-gas sensor for environmental monitoring. *Appl. Opt.* **2007**, 46, 8202-8209.
11. Risby, T.H.; Tittel, F.K.; Current status of midinfrared quantum and interband cascade lasers for clinical breath analysis. *Optical Engineering* **2010**, 49, 111123.
12. Soibel, A.; Wright, M.W.; Farr, W.H.; et al. Midinfrared Interband Cascade Laser for Free Space Optical Communication. *IEEE Photonics Technology Letters* **2010**, 22, 121-123.
13. Yang, R.Q.; Li, L.; Jiang, Y.C.; Interband cascade laser: from original concept to actual device. *Progress in Physics* **2014**, 34, 169-190.
14. Deng, Y.; Zhao, B.B.; Wang, C.; Linewidth broadening factor of an interband cascade laser. *Applied Physics Letters* **2019**, 115, 181101.
15. Deng, Y.; Fan, Z.F.; Wang, C.; Optical feedback induced nonlinear dynamics in an interband cascade laser. *Proc. Of SPIE* **2021**, 11680, 116800J.
16. Panajotov, K.; Sciamanna, M.; et al. Optical Feedback in Vertical-Cavity Surface-Emitting Lasers. *IEEE Journal of Selected Topics in Quantum Electronics* **2013**, 19, 1700312.
17. Yang, R.Q.; Mid-infrared interband cascade lasers based on type-II heterostructures. *Microelectronics Journal* **1999**, 30, 1043-1056.
18. Lang, R.; Kobayashi, K.; External optical feedback effects on semiconductor injection laser properties. *IEEE Journal of Quantum Electronics* **1980**, 16, 347-355.
19. Deng, Y.; Wang, C.; Rate Equation Modeling of Interband Cascade Lasers on Modulation and Noise Dynamics. *IEEE Journal of Quantum Electronics* **2020**, 56, 2300109.
20. Bewley, W.W.; Lindle, J.R.; Kim, C.S.; et al. Lifetimes and Auger coefficients in type-II W interband cascade lasers. *Applied Physics Letters* **2008**, 93, 041118.
21. Vurgaftman, I.; Canedy, C.L.; Kim, C.S.; et al. Mid-infrared interband cascade lasers operating at ambient temperatures. *New Journal of Physics* **2009**, 11, 125015.

22. Vurgaftman, I.; Bewley, W.W.; Canedy, C.L.; Chul Soo Kim; Mijin Kim; Lindle, J.R.; Merritt, C.D.; Abell, J.; Meyer, J.R.; Mid-IR Type-II Interband Cascade Lasers. *IEEE Journal of Selected Topics in Quantum Electronics* **2011**, 17, 1435–1444.
23.
24.
25.